CrossMark

**RESEARCH PAPER**

# Hydrogen degradation effects on mechanical properties in T24 weld microstructures

Michael Rhode[1] · Joerg Steger[1,2] · Thomas Boellinghaus[1] · Thomas Kannengiesser[1]

**Abstract** Spectacular failure cases of fossil power stations in the recent years exhibited severe cracking in T24 welds. The results show that hydrogen-assisted cracking up to 200 °C cannot be excluded. Hence, it is important to gain a basic understanding on how hydrogen might affect the basic material properties in the respective weld microstructures. The present study focuses on hydrogen degradation of the respective weld microstructures, i.e., the weld metal and the coarse grained heat affected zone, where actually cracking appeared in practice. Tensile tests were carried out for coarse grain heat-affected zone (CGHAZ) and the weld metal in uncharged and electrochemically hydrogen-charged condition. It turned out that both microstructures show distinct tendency for gradual degradation of mechanical properties in the presence of increasing hydrogen concentration. Already for a hydrogen concentration about and above 2 ml/100 g Fe, a significant ductility reduction has been observed. SEM investigations revealed that the fracture topography changes from ductile topography in uncharged condition to intergranular topography for the CGHAZ and to ductile-brittle mix for the weld metal (WM) in hydrogen charged condition. Ti-rich inclusions were identified as central regions of quasi-cleavage fracture areas in the WM. An approximation procedure is applied to quantify the degradation intensity.

✉ Michael Rhode
michael.rhode@bam.de

1 BAM Federal Institute for Materials Research and Testing, Berlin, Germany

2 Otto von Guericke University, Magdeburg, Germany

## 1 Introduction

Safety and reliability of weld joints are important facts for the later operating of welded components. A particular example is represented by high-strength Cr-Mo-V steels with high long-term creep resistance which are widely used in fossil fuel operated power stations (coal and gas), particularly for boiler components like water wall panels [1–3]. An appropriate material candidate was the bainitic low alloyed steel grade T24 (7CrMoVTiB10-10) combining the effects of lower manufacturing costs due to low alloy concept and improved creep resistance by addition of Ti, V, or B. Additionally, the weldability of the T24 was improved in terms of the avoidance of the post-weld heat treatment (PWHT) for thin-walled components with $t < 10$ mm [1, 2] due to the decreased carbon content resulting in a maximum hardness of 350 HV. Nevertheless, creep-resistant steels like the T24 can show a possible hydrogen absorption during welding or later service-conditions resulting in a certain susceptibility for hydrogen-assisted cracking (HAC) or the general degradation of the mechanical properties [4, 5]. It is well-known that this susceptibility is influenced by the material strength as well as the chemical composition. In the case of the T24, the Vanadium-addition increases the hydrogen solubility of the material due to V-rich precipitations (carbides) or V as substitution atom in the lattice [6–8].

Spectacular failure cases of fossil power station components (water wall panels) in the recent years exhibited severe cracking in the tubular welds [9] mainly in the root regions of the weld or in the HAZ. Since the first failures occurred, an

Springer

ongoing discussion started including metallurgical facts, welding technique, and power plant start-up procedures. As example, anodic stress corrosion cracking (SCC) occurred in high temperature water in the presence of oxygen between 150 and 280 °C [10] and was assumed as initial point for cracking process. In contrast to currently further otherwise undertaken speculations [11, 12], hydrogen-assisted (stress corrosion) cracking in the higher temperature regime of up to 200 °C cannot be excluded [13], particularly not in those cases when newly manufactured boilers underwent numerous cycling through this temperature range during the start-up process. As example, Hoffmeister and Böllinghaus reported that the highest cracking sensitivity occurred under laboratory condition in distilled water at a temperature of 200 °C [13]. This is in accordance to observations in nuclear power plants under simulated hot water environment. In this case, hydrogen-assisted SCC occurred even in the absence of hydrogen promoters in deionized water [14]. Relatively early in 2005, the T24 weld metal (WM) without PWHT was reported with a potential higher susceptibility for HAC compared to the HAZ [15]. Additionally, Mohyla and Foldyna reported that PWHT is necessary in the case of T24 due to possible secondary hardening effects after exposure to elevated operating temperatures [16]. The referred literature suggests the increased HAC susceptibility of the T24 weld microstructures. This can be attributed to the complex structure and precipitation of the appearing (V, Ti, or B−) carbides or nitrides as well as the tempering influence of an additionally applied PWHT in the HAZ as well as the weld metal. Hence, the possible weld microstructure influence should be considered for the HAC susceptibility in the temperature range up to 200 °C (start-up procedures).

In general, HAC (or degradation of the mechanical properties) occurs under the interaction of the local hydrogen concentration, local mechanical load, and the specific microstructure, i.e., HAC occurs in a specific microstructure, if the local mechanical load exceeds the critical value at a specific hydrogen concentration, generally at temperatures below 200 °C. A critical combination of these factors can be influenced by different microstructure features like the grain size or the size and the orientation of precipitates. Thus, different studies showed the general tendency of hydrogen influenced degradation of the ductility compared to the less affected strength with increasing hydrogen concentration [17, 18]. Hence, a decrease of the ductility (described by elongation at failure or reduction in area) dependent

on a hydrogen concentration is suitable for describing the HAC susceptibility like the authors did in another study for high-strength low alloyed steels [19].

Due to the mentioned facts, it is important to gain a basic understanding how hydrogen might affect the basic material properties in the respective weld microstructures. The present study focuses on hydrogen degradation of the respective weld microstructures, i.e., the WM and the coarse-grained heat affected zone (CGHAZ), where actually cracking appeared in practice in 2010. CGHAZ microstructure was thermally simulated from T24 base metal specimens. Subsequently, round tensile specimens were machined. Pure weld metal tensile specimens were machined from manually TIG-welded butt joints. Thus, similar welding parameters were applied as for the real on-site weld joints, i.e., those welds which failed during the in-service operation of the plant boilers. For the subsequent hydrogen charging, an electrochemical charging method was applied.

## 2 Materials and methods

Two different microstructures were examined with hydrogen-free and hydrogen-charged tensile specimens. First, the coarse-grained heat-affected zone (CGHAZ) was examined and second the weld metal (WM).

### 2.1 Material

As base material (BM), the creep resistant low-alloyed steel T24 (7CrMoVTiB10-10) was used, and the CGHAZ was weld-simulated by the specific thermal cycles given further below. To produce the needed weld metal specimens, a commercially available filler material was used (welding rods for manually TIG welding). The chemical composition of the base and weld metal is given in Table 1, and the obtained mechanical properties (uncharged condition) of the CGHAZ and weld metal are shown in Table 2.

**Table 1** Chemical composition of T24 and weld metal (wt%)

| Grade | C | Cr | Mo | V | Ti | B | P + S |
|---|---|---|---|---|---|---|---|
| BM/CGHAZ | 0.080 | 2.440 | 1.000 | 0.264 | 0.070 | 0.005 | 0.001 |
| WM | 0.070 | 2.520 | 1.000 | 0.260 | 0.035 | 0.002 | 0.001 |

**Table 2** Mechanical properties of CGHAZ and WM

| Grade | Rp0,2 in MPa | Rm in MPa | A in % |
|---|---|---|---|
| CGHAZ | 856 | 1137 | 15 |
| WM | 727 | 950 | 17 |
| BM (comparison) | 590 | 673 | 22 |

## 2.2 Weld metal

The plates were welded manually TIG-welded. For reproducible results, the welds were carried out in PA position at on sheet metal with a plate thickness of 7.1 mm. Figure 1 shows the used weld geometry and the location of the longitudinal tensile specimens.

The welds were carried out by three layers. Table 3 shows the used welding parameters. The weld seam length was 160 mm.

The typical microstructure of the welds is shown in Fig. 2 and exhibited a typical bainite microstructure, as common for this type of steels. By respective measurements, it was ascertained that the Vicker's hardness in these weld metals did not exceed 350 HV [1, 2]. The measured average hardness of the WM ranged about 300HV10. For comparison to real in-field component weld joints, the weld WM tensile specimens were machined from the plates in "as-welded" condition without PWHT (post-weld heat treatment). Each weld seam was subjected to nondestructive X-ray inspection for avoiding failures like cracks or inclusions in the specimens prior to machining the specimens.
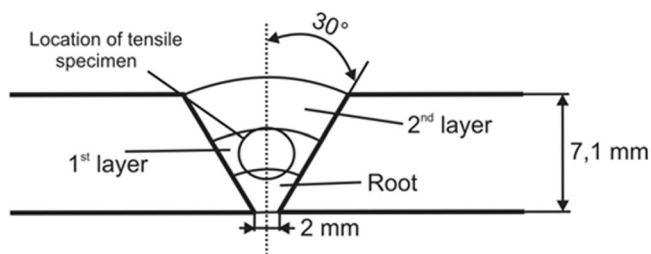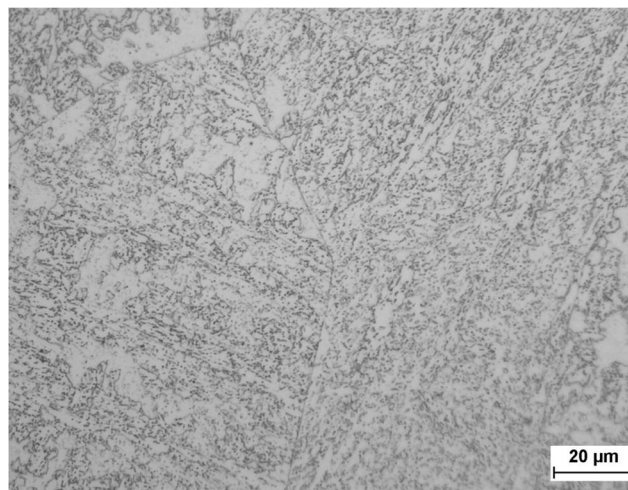


**Fig. 2** Magnified weld metal

## 2.3 Weld-simulated CGHAZ

For a homogeneous CGHAZ microstructure, T24 base metal round bars with the dimensions of 80-mm length and 6-mm diameter were heat-treated by inductive heating to a peak temperature of 1200 °C and then cooled down under controlled nitrogen gas flow for fixed $t_{8/5}$ time of 5 s. The temperature was measured using a Sensortherm Metis QP22 pyrometer and simultaneously recorded via PC work station. Metallographic longitudinal and cross sections were made to ensure homogenous microstructure of the CGHAZ specimens in the gauge length of the tensile specimens. The metallographic cross section of the CGHAZ shows a mostly martensitic structure (Fig. 3). The obtained hardness



**Fig. 1** Weld geometry

**Table 3** Welding parameters

| Parameter | Root | First layer | Second layer |
|---|---|---|---|
| Voltage in V | 16 | 19 | 19 |
| Current in A | 90 | 120 | 120 |



**Fig. 3** Magnified CGHAZ

of the simulated coarse grained zone is about 300HV10 as well as for the WM. The selected $t_{8/5}$ time was chosen in accordance to recommendations of continuous TTT curve for T24 [20] and because of the requested martensite formation in the CGHAZ (assessing as "worst-case" scenario) because martensite is known for increased degradation of mechanical properties in the presence of hydrogen compared to the bainitic microstructures [21]. As compared to weld metal, the CGHAZ is in "as-welded" condition without additional post-weld heat treatment.

## 2.4 Hydrogen charging

The hydrogen charging was performed with cathodic charging procedure using 0.1-M $H_2SO_4$ acid solution with addition of 12 mg/l $NaAsO_2$ as recombination poison to prevent the hydrogen from recombination to molecular form. The galvanostatic charging (constant current density during charging) was used to obtain different hydrogen concentrations by varying the charging current density. Before charging, each specimen was cleaned in acetone using an ultrasonic bath and rinsed in inert nitrogen gas flow. By respective preexperiments, it was ensured that cylindrical CGHAZ and WM calibration specimens (3-mm diameter, 20-mm length) experience full-hydrogen saturation. The following Table 4 shows the used parameters for hydrogen charging.

The saturation of the specimens was ensured for each parameter set with additional charged specimens. Thus, they were exposed to the electrolyte solution for the mentioned times in the Table 4 plus ten additional hours. Subsequently, the achieved hydrogen concentrations of both charging times were compared (i.e., 24 and 34 h).

The obtained results showed that the corresponding hydrogen concentrations only varied ±10 %. Hence, the mentioned times given in brackets in Table 4 are intended to be sufficient for hydrogen charging.

**Table 4** Charging parameters

| Grade | Charging current density in mA/cm$^2$ | | |
|---|---|---|---|
| | Level I | Level II | Level III |
| CGHAZ | 1.5 (16 h) | 1.5 (24 h) | 10 (24 h) |
| WM | 0.5 (24 h) | 1.3 (24 h) | 3.75 (24 h) |

## 2.5 Tensile testing

Tensile tests were performed to determine the hydrogen degradation effect on the mechanical properties. An Instron 8520 test facility was used with an elongation rate of 1 mm/min. The yield strength (YS, $R_{p0.2}$) and ultimate tensile strength (UTS, $R_m$) were recorded. The elongation was measured with a clip strain gauge during testing. All data were captured and stored with a triggered data logging system. After the tensile test, the reduction in area was determined using optical microscopy with five times magnification and a digital image capture system. After charging, the specimens were stored immediately in liquid nitrogen at −196 °C to prevent the hydrogen from effusing until the tensile test. Before testing, each specimen was defrosted in acetone for ca. 60 s to achieve ambient temperature. Conducted previous experiments showed that an average hydrogen loss occurs 10 to 15 % after stop of hydrogen charging, tensile testing, and final hydrogen determination in the hydrogen analyzer. Figure 4 shows the used round tensile specimen geometry.

After the tensile test, one half of the fractured specimen was stored in liquid nitrogen at −196 °C again for the later analysis of the corresponding hydrogen concentration in the specimen. The other half of the specimen was used for fractography analysis by scanning electron microscope (SEM).

## 2.6 Hydrogen detection

The corresponding hydrogen content in the specimens was measured using a Bruker JUWE H-mat 221. This device uses the carrier gas hot extraction technique with thermal conductivity device (TCD) to determine the effusing hydrogen from the specimens. Thus, the specimen is heated up in a glass plunger in inert gas flow (nitrogen). The effusing hydrogen changes the thermal conductivity of the inert gas and is recorded with the TCD sensor. The calibration with different defined amounts of hydrogen volumes allows the calculation of a regression function for the correlation of the TCD values and a corresponding hydrogen amount [22, 23].

Before the hydrogen analysis is started, the specimen is removed from the liquid nitrogen and the head of the fractured tensile specimen (in accordance to the geometry in Fig. 4) is cut by a bolt cutter in frozen condition from the test range of the tensile specimen (3-mm diameter and corresponding length to fracture in average 10 mm). Immediately after, the residual cut hydrogen-charged tensile specimen volume is weighed in frozen condition, and the weight is transferred to the hydrogen analyzer for starting analysis. During start-up of the experimental equipment (heating of the infrared furnace), the specimen is defrosted for 60 s in ethanol to ambient

**Fig. 4** Tensile specimen geometry
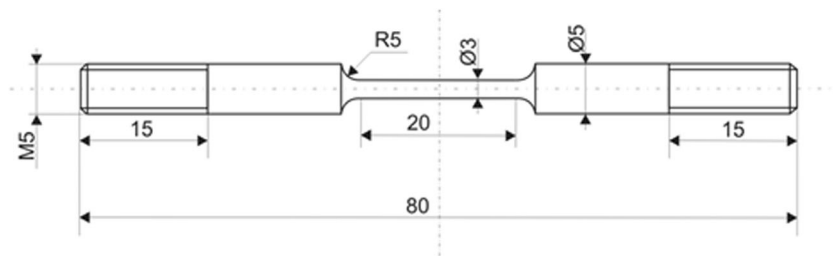


temperature. Then, the specimen is inserted in the glass plunger and hydrogen collection starts. After hydrogen analysis, the tested specimen is weighted again. Thus, this determined reference weight is applied for the calculation of the corresponding hydrogen concentration. Previous experiments with the mentioned calibration specimens (of the hydrogen charging tests) were subjected to different testing temperatures. It was obtained that the hydrogen amount in the specimen was similar between a testing temperature of 200 and 800 °C. Temperatures below 200 °C could not be examined with the presented hydrogen analyzer due to the limited resolution of the TCD sensor. This means that possible hydrogen trapping effects up to 200 °C have to be neglected and the temperature for hydrogen collection was set 800 °C for accelerated hydrogen collection. Additionally, setting the temperature to 800 °C allows improved hydrogen collection due to higher effusion rates which allow better accuracy of the TCD.

In general, the time from removing the specimen from the liquid nitrogen until hydrogen collection was approximately 130 s.

## 3 Results and discussion

### 3.1 Hydrogen solubility

Different charging current densities were used to obtain different hydrogen concentrations in the tensile specimens. The coarse grained zone shows a smaller solubility for hydrogen than the weld metal. Table 5 shows the obtained results for the

CGHAZ and weld metal in accordance to the charging parameters given in Table 4.

The performed charging tests showed that hydrogen concentration reached a maximum value of 4.5 ml/100 g Fe for the CGHAZ and 9 ml/100 g Fe for CGHAZ. Coudreuse et al. [24] used high-pressure gas phase charging and determined a hydrogen solubility of approximately 3 ml/100 g Fe for conventional Cr-Mo steels and 5 ml/100 g Fe for V-modified steel grades. Brass et al. [25] used electrochemical charging procedure for hydrogen charging and reported a hydrogen solubility of 2.3 ml/100 g Fe for conventional 2.25V-1Mo steel grade and 4.4 ml/100 g Fe (4 wt ppm) for a 3Cr1MoV steel grade. In general, the reported hydrogen solubility of V-added Cr-Mo steels is higher compared to conventional Cr-Mo grades due to the addition of V, as example in terms very fine dispersed $V_4C_3$ carbides as reported by Takahashia et al. [26]. The obtained maximum hydrogen concentration of ~4.5 ml/100 g Fe for the T24 CGHAZ is in agreement to the previous mentioned reference. The higher hydrogen solubility of the WM can be influenced by the tempering effect of the three-layer technique (as shown in Fig. 1, the WM specimens were extracted from the second layer). An additional tempering was reported by Depover et al. [27] for laboratory casts of Fe-C-X (X = Ti, Cr, or Mo) resulting in an increased capability for hydrogen trapping due to the forming carbides. In contrast, Parvathavarthini et al. reported [28] that a tempering results in a lower hydrogen solubility due to the annihilation of dislocations (acting as reversible hydrogen traps). Additionally, the dissolution of the carbides in the CGHAZ suggests an increasing number of solute Cr, Mn, or V atoms in the lattice acting as reversible hydrogen traps [29]. Nevertheless, the observed hydrogen solubility of the CGHAZ is lower compared to the (tempered) WM. The influence of (prior austenite) grain boundaries in the HAZ on the hydrogen solubility can be both: decreasing or increasing [30]. But in accordance to Liu et al. [31], grain boundaries (i.e., the grain size) cannot be separated as predominantly hydrogen trap if other effects appear at the same time like dissolution of precipitates/carbides in terms. This is especially the case if

**Table 5** Hydrogen concentration in CGHAZ and weld metal

| Grade | Hydrogen concentration in ml/100 g Fe | | |
|---|---|---|---|
| | Level I | Level II | Level III |
| CGHAZ | ~2.0 | ~2.0 | ~4.5 |
| WM | ~3.0 | ~5.0 | ~9.0 |

HAZ is formed during welding in the BM. Hence, the microstructure features like precipitates or inclusions play an increased important role and demonstrate that each microstructure should be investigated separately in terms of the solubility and, hence, the mechanical properties.

### 3.2 Mechanical properties CGHAZ and WM

During tensile test, the test force and the elongation were recorded (for specimens that fractured in the gauge length of the extensometer). The corresponding ultimate tensile strength $R_m$ (UTS) and the yield strength $R_{p0,2}$ (YS) were calculated. The reduction in area was determined by measuring the fracture surface area by optical microscope with ×5 magnification. In general, the mechanical properties of the microstructures showed a similar behavior. With increasing hydrogen concentration, there is a distinct degradation of the mechanical properties especially the ductility (expressed by elongation at failure and reduction in area).

#### 3.2.1 CGHAZ

Figure 5 shows the determined values of $R_{p0.2}$ and $R_m$ (YS and UTS) dependent on the hydrogen concentration measured in the gage length for the CGHAZ microstructure, respectively. The figures after Fig. 5 show the obtained results for the hydrogen influenced ductility: expressed by elongation at failure (Fig. 6) and reduction in area (Fig. 7).

As can be drawn from Fig. 5, the UTS and YS of the CGHAZ are not significantly affected by hydrogen up to a hydrogen concentration of 2 ml/100 g Fe. In uncharged condition, the UTS is about 1130 MPa (YS about 850 MPa). Up to 2 ml/100 g hydrogen concentration, the UTS slightly decreases to 1100 MPa. In the same hydrogen concentration
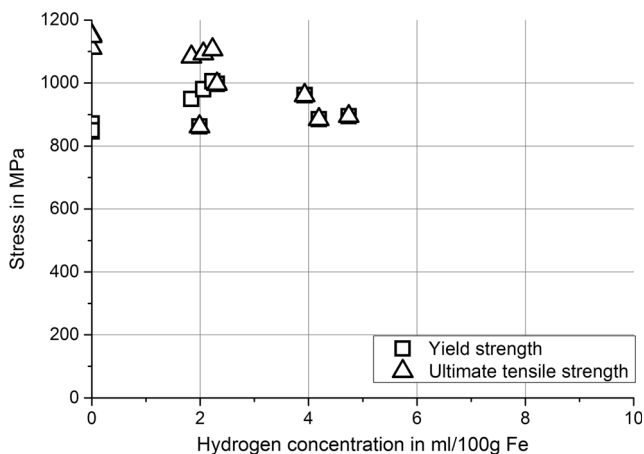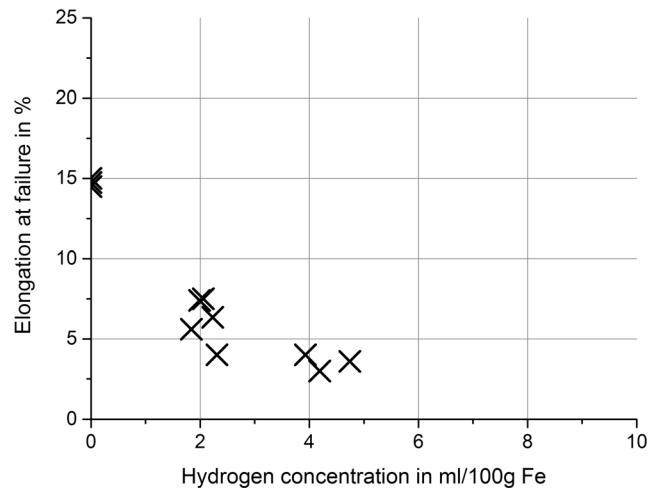


**Fig. 6** Elongation at failure of CGHAZ

range, a more pronounced increase of the YS has been observed (increases from 850 MPa to approximately 950 MPa). Such effects of hydrogen on the strength values can be observed for quite a number of bcc steels [21, 32]. It is generally anticipated [33] that hydrogen, located at the interstitial places in the matrix, blocks dislocations and retards slipping during straining (so-called hydrogen enhanced localized plasticity (HELP)). After exceeding the hydrogen concentration of 2 ml/100 g Fe, a distinct decrease of the UTS below 1000 MPa was observed. Over a larger range of obtained hydrogen concentration, the UTS equals to YS. In other words, distinct hydrogen related degradation of UTS and YS occurs above this hydrogen concentration and the susceptibility for HAC increases. The maximum hydrogen charging was up to 4.5 ml/100 g Fe (corresponding to 10 mA/cm² charging current density for hydrogen charging). Unfortunately, larger
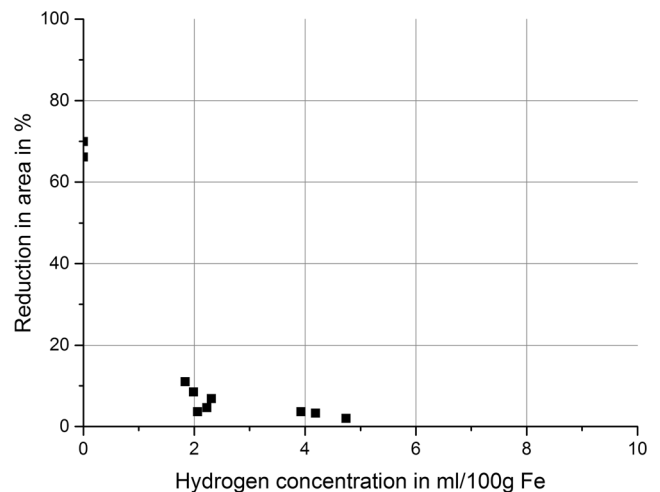


**Fig. 5** YS and UTS for CGHAZ



**Fig. 7** Reduction in area of CGHAZ

hydrogen concentrations could not be realized in the specimens due to avoidance of internal precracks or surface defects like blisters, although it is expected that YS and UTS would be reduced much more with higher hydrogen concentrations. On the other hand, larger hydrogen concentration values than 4.5 ml/100 g seem quite unrealistic.

Additional to the UTS and YS, the elongation at failure was determined for the CGHAZ and is given in Fig. 6. In general, the elongation at failure decreases with increasing hydrogen concentration. In uncharged condition, the elongation is about 15 %. As described before, there is a distinct loss of the elongation (to fracture) when reaching a hydrogen concentration of ~2 ml/100 g Fe. Up to this hydrogen concentration, the elongation decreases from 15 to 5 %. Additional to the elongation at failure, the reduction was determined for the CGHAZ tensile specimens by investigation with light microscope using image capturing program. The determined data is presented in Fig. 7.

In uncharged condition, the reduction in area is about 68 %. The charged specimens with a hydrogen concentration of ca. 2 ml/100 g Fe showed a decrease to 5 to 10 %. In other words, there is distinct loss ductility (as determined with the elongation at failure respectively). If the hydrogen concentration is increased to 5 ml/100 g Fe, the reduction in area decreases below 10 %. It is obvious that the increasing hydrogen concentration increases the degradation and the potential risk of a failure (e.g., HAC). This is in accordance to reported literature assuming the CGHAZ of Cr-Mo-V weld microstructures as most susceptible microstructure to HAC [8, 13].

### 3.2.2 WM

Previous tests with the calibration specimens showed that lower current densities lead to higher absorbed hydrogen concentration in the WM compared to the CGHAZ (see Sect. 3.1). Due to the higher possible hydrogen concentration in the WM, the charging parameters (current density and charging time) were adapted. It is assumed that the WM microstructure can solute more hydrogen in the bulk due to the increased number of hydrogen trap sites like voids or solute atoms and especially a changed number and density of carbides in the WM compared to the CGHAZ. The reason is assumed to be the tempered microstructure of the WM (due to the multilayer welding) compared to the as-quenched CGHAZ resulting in increased number of carbides acting as hydrogen traps [27–29]. This can be also seen in the distinct quasi-cleavage fracture around Ti-rich inclusions in the case of the WM (see Figs. 17 and 18). As already mentioned [30, 31], a possible grain size influence cannot be separated if effects like carbide dissolution or tempering effects occur like in the case of the conducted three-layer welding. Hence, a simple reason for the

increased hydrogen solubility of the weld metal cannot be given. It was possible to charge the weld metal up to approximately 9 ml/100 g Fe. Additionally, the solubility is a secondary result derived from the mechanical tests. Hence, the degradation of the mechanical properties is in the main focus of this study. To get reproducible results, a well as to avoid surface damage like blistering electrochemical charging was performed with a maximum charging current density of 3.75 mA/cm$^2$. Figure 8 shows the determined mechanical properties (UTS and YS).

As shown in Fig. 8, the strength of the WM is more or less unaffected by increasing hydrogen concentrations. In the uncharged condition, the UTS is about 950 MPa and the YS is about 730 MPa. These obtained values are in agreement for the WM without PWHT as reported in [34]. Compared to the CGHAZ, the UTS and YS of the WM are lower. From this point of view, the CGHAZ is assumed to be more susceptible to hydrogen-related degradation of mechanical properties in the presence of hydrogen in the material.

A similar loss of the ductility was determined for the WM as well as the CGHAZ (Fig. 9). In contrast to the ultimate tensile strength (UTS) or yield strength (YS), the elongation at failure of the WM is significantly affected by hydrogen. It is obvious that even small hydrogen concentration up to 1 ml/100 g Fe can decrease the total elongation from approximately 15 % in uncharged condition (average value) to approximately 10 %. After exceeding hydrogen concentration 1 ml/100 g Fe, the elongation at failure is below 5 %. As shown for the CGHAZ, Fig. 10 indicates the determined reduction in area for the WM.

Similarly to the elongation at failure for the WM (Fig. 9), also the reduction in area decreases distinctly with increasing hydrogen concentration compared to the UTS and YS. The uncharged condition shows approximately 78 % and equals to high ductility (small diameter after fracture). If charged with a
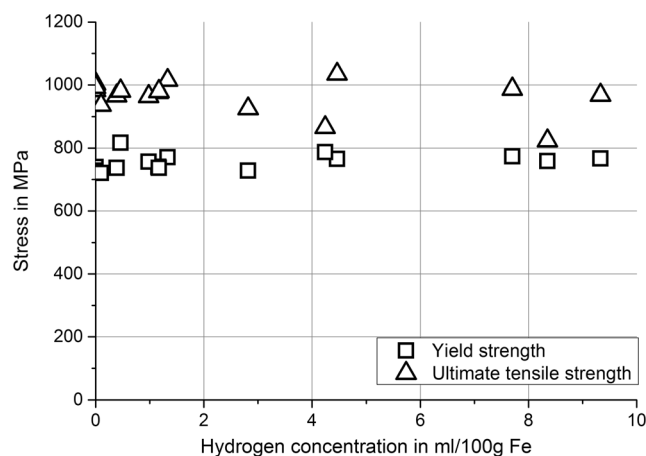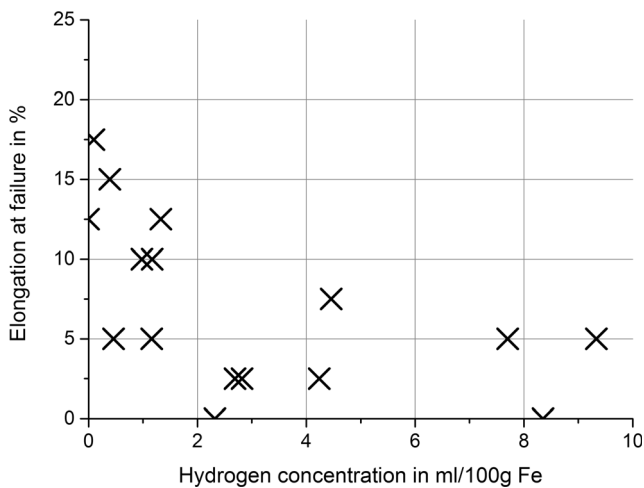


**Fig. 8** UTS and YS for WM

**Fig. 9** Elongation at failure of WM

hydrogen concentration of 1 ml/100 g Fe, the reduction in area decreases to about 30 % and is below 10 % when charged with higher hydrogen concentrations. Blach et al. [17] reported for electrochemically charged T24 weld metal notched tensile specimens a distinct loss in ductility too, but they did not give corresponding hydrogen concentrations. But, they conclude the increase of the degradation with increasing hydrogen concentration which is in close agreement to our study. Additionally, hydrogen-related degradation maybe influenced by the applied strain rate due to necessary time for hydrogen diffusion into highly strained regions for crack propagation. In our study, the strain rate equals $8.3 \times 10^{-4}$ $1*s^{-1}$. But, Xu et al. [35] reported for 40 times lower strain rate ($2.0 \times 10^{-5}$ $1*s^{-1}$), a decrease of the reduction in area to 30 % for tempered Cr-Mo-steel at hydrogen concentration of 1 ppm (1.1 ml/100 g Fe) which is in close agreement to our obtained data. The determined reduction in area suggests an increased degrada-
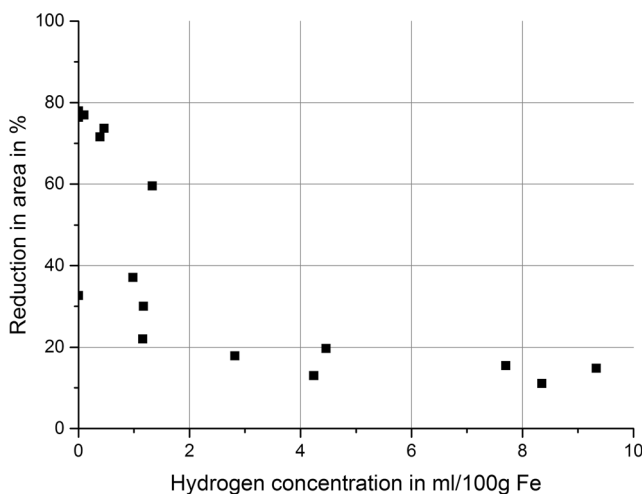
tion of the WM expressed by distinct loss of ductility. Compared to the tensile properties (UTS and YS), the elongation at failure or reduction in area is assumed to be suited as assessment parameter for degradation of mechanical properties.

The obtained mechanical data (hydrogen charged vs. the hydrogen free condition) can be applied as qualitative assessment parameter for the evaluation of the degradation intensity. It is quite noteworthy that the CGHAZ shows at a hydrogen concentration of 4.5 ml/100 g a distinct degradation of UTS and YS, while the WM is mostly unaffected and this at even higher concentrations of up to 9 ml/100 g. Due to the well-known [18, 19, 21] fact that hydrogen degrades more in terms of the ductility than the strength of a material, both microstructures show significant hydrogen-related degradation of ductility (expressed by elongation at failure and reduction in area). A relatively low hydrogen concentration of 2 ml/100 g Fe remarkably decreases the load capacity of both examined microstructures and has to be considered in the case of welding fabrication.

### 3.3 Degradation intensity

To rank the intensity of the hydrogen effect to the degradation, the so-called embrittlement index EI was used. The calculation of this index is defined in Eq. 1: Embrittlement index, as example according Xu et al. [35] or to Depover et al. [36]:

$$EI = 1 - \frac{RA_u - RA_c}{RA_u} \tag{1}$$

With EI as embrittlement index, the reduction in area $RA_u$ in % for uncharged condition and the reduction in area $RA_c$ in % for hydrogen charged condition. The next figures show the calculated embrittlement index for the CGHAZ (Fig. 11) and the WM (Fig. 12).
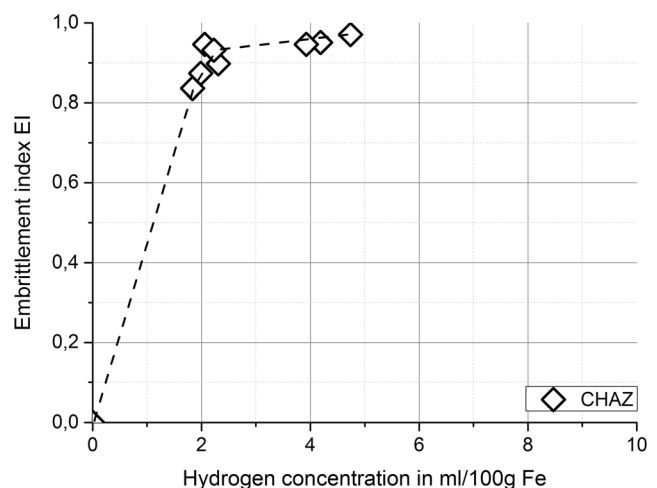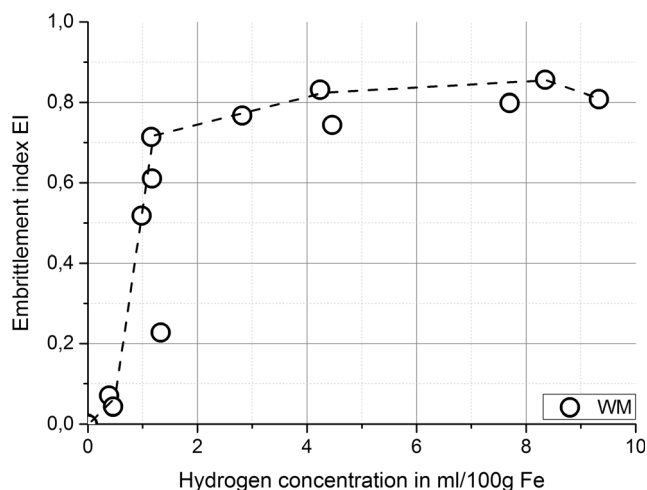


**Fig. 10** Reduction in area of WM



**Fig. 11** Embrittlement index of CGHAZ

Fig. 12 Embrittlement index of WM



Fig. 13 CGHAZ uncharged

Obviously, with increasing hydrogen concentration, the hydrogen embrittlement index (EI) and the hydrogen susceptibility increase for both microstructures. Referred to Fig. 11, the CGHAZ shows a slight higher degradation effect compared to the WM. This is due to the qualitative higher calculated embrittlement index *EI* of the CGHAZ (approximately 0.85 at hydrogen concentration of 2 ml/100 g Fe) compared to the WM (approximately 0.71 at hydrogen concentration of 2 ml/100 g Fe).

### 3.4 Fractography

The occurred fracture surfaces for both microstructures were examined by scanning electron microscope (SEM) with additional EDX analysis to identify the chemical composition of potential inclusions. Figures 13 and 14 show the fracture surface of the uncharged CGHAZ specimen and of a specimen with a relatively high hydrogen concentration, respectively.

For the uncharged condition (Fig. 13), the fracture topography is mostly ductile characterized by typical dimples (marked with "D") as known as micro void coalescence. The well-known typical dimpled structure distinguishes this fracture topography and initiates as example at secondary phase particles like inclusions or precipitates [37–39].

It becomes obvious by the different photographs that with increasing hydrogen concentration, the fracture topography of the CGHAZ changes. If the tensile specimens are charged with a medium hydrogen concentration of approximately 2 ml/100 g Fe (Fig. 14), distinct cleavage fracture occurs in the biggest part of the surface area (marked with "CF"). This behavior corresponds to the determined loss of ductility in the CGHAZ at this hydrogen concentration. The CF condition is indicated by typi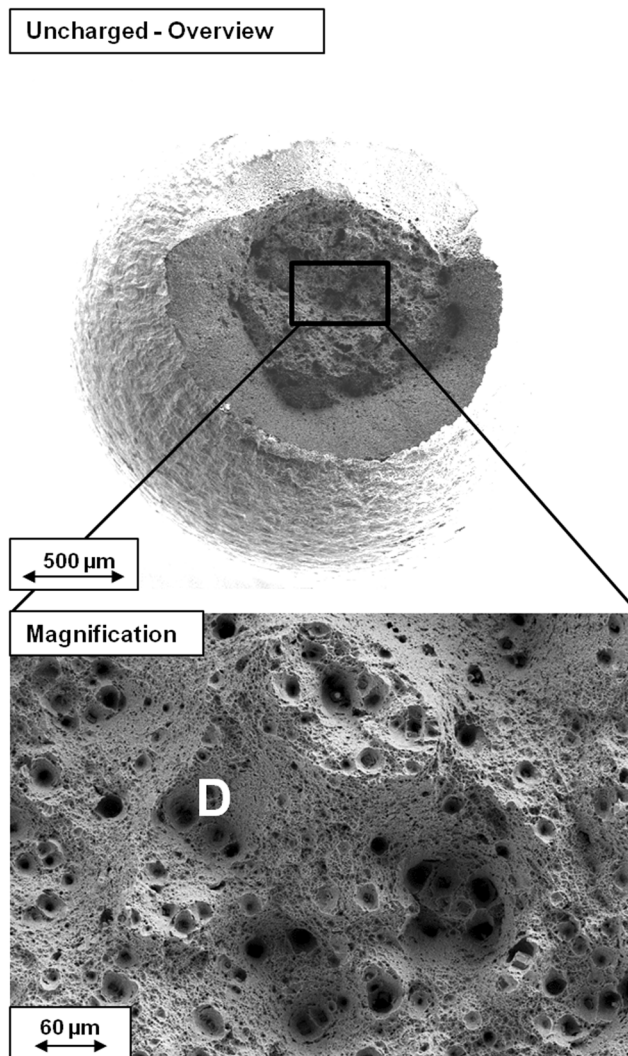cal transgranular fracture with smooth cleavage facets (as shown in the lower part of Fig. 14). At relatively high hydrogen concentration of 4.5 ml/100 g Fe (Fig. 15), intergranular cracking topography appears (indicated with "IG"). Additionally, secondary cracks appeared (indicated with "SC") between the grains in transverse direction to the loading direction. As marked with red dashed lines in the upper part of Fig. 15, the major part of the fracture surface is covered by intergranular rupture. This change of the fracture topography is in accordance to the determined significant loss of the mechanical properties (UTS and YS) and the ductility, respectively.

In the relatively high hydrogen charged condition (above 2 ml/100 g Fe), the determined changing fracture topography (cleavage cracking and intergranular cracking vs. dimpled structure of the hydrogen free condition) is a typical sign for hydrogen-assisted degradation of the mechanical properties in
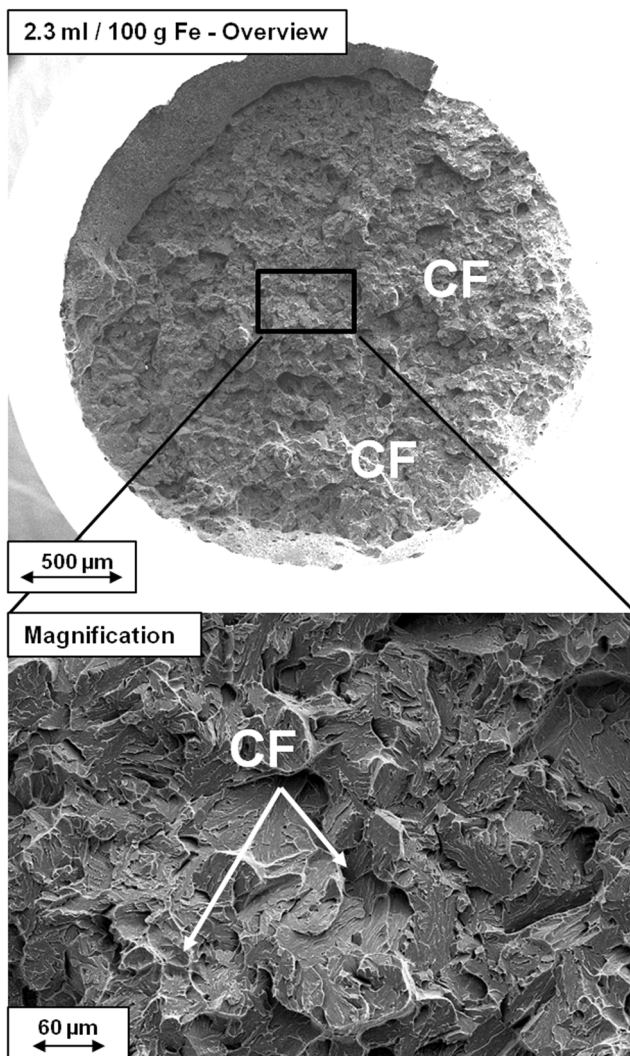
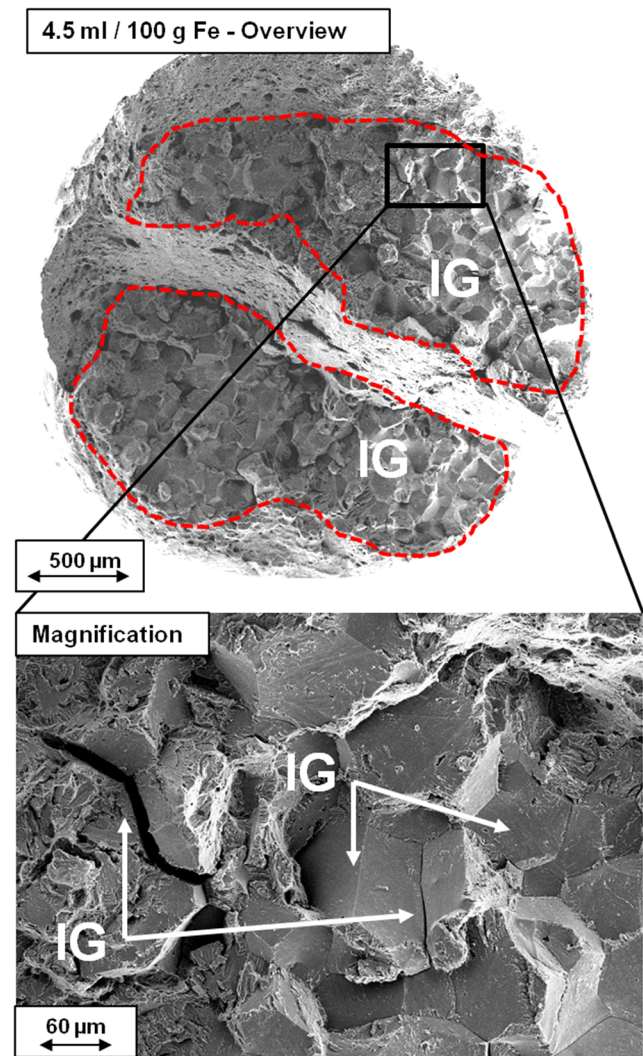**Fig. 14** CGHAZ charged with 2.3 ml/100 g Fe



**Fig. 15** CGHAZ charged with 4.5 ml/100 g Fe

terms of ductility [18, 40]. From the point of component safety, it can only be emphasized that a hydrogen concentration of approximately 2 ml/100 g Fe already entails a significant degradation of ductility and should be avoided during welding fabrication of T24 components which are subjected to CGHAZ formation as a consequence of welding without PWHT.

A similar behavior was determined for the weld metal (WM). Figures 16 to 19 show the uncharged condition and hydrogen charged condition in increasing order of hydrogen concentration.

As shown in Fig. 16, for the uncharged condition, there was also ductile fracture topography determined for the WM as compared to the CGHAZ (also marked with "D"). In hydrogen charged condition, the WM shows a changed dominant fracture compared to the CGHAZ.

Already at hydrogen concentration of 1 ml/100 g Fe, the fracture topography of the WM changes from almost ductile to a mixture of quasi-cleavage fracture topography (marked with "C in white dashed lines") and ductile dimpled structure as shown in Fig. 17. In contrast to the pure cleavage fracture "CF," the quasi-cleavage fracture "C" is indicated by transgranular fracture but with noncleavage planes labeled with fine lines called "river markings" [41, 42]. In accordance to Lynch [41] and Martin et al. [42], the "C"-fracture topography indicates a typical hydrogen-affected fracture topography. With further increased hydrogen concentration (Fig. 18 - 4.5 ml/100 g Fe), the dominant fracture topography is the mentioned mixture of quasi-cleavage cracking ("C") and ductile dimples ("D").

In general, the total "embrittled" area increases quantitatively. This is in accordance to the distinct loss of
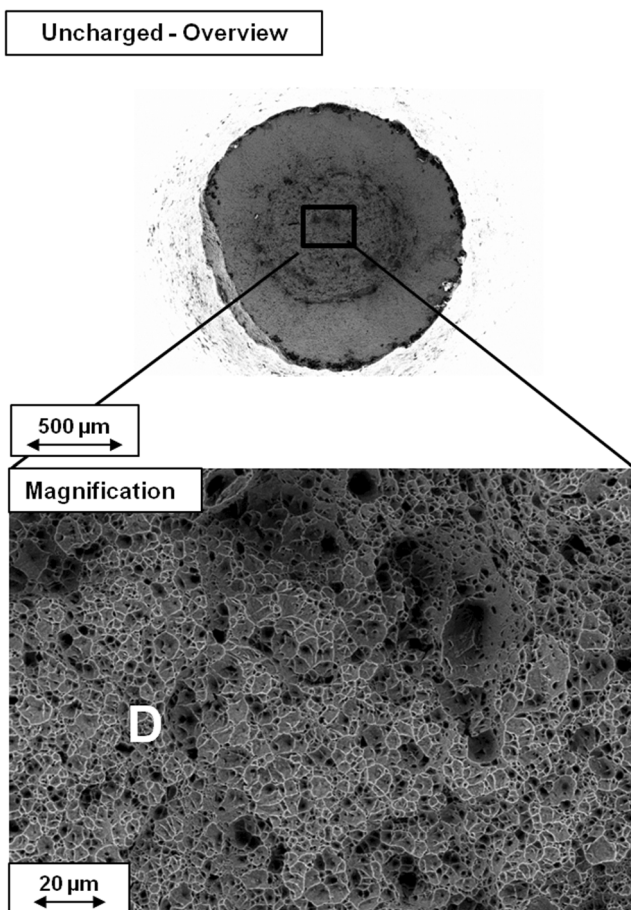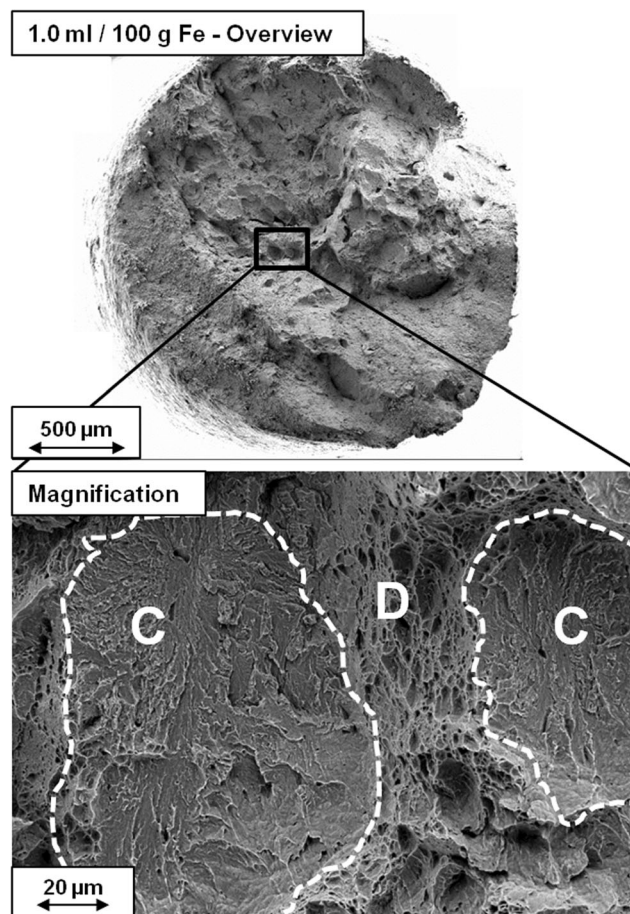
Fig. 16 WM uncharged



Fig. 17 WM charged with 1.0 ml/100 g Fe

ductility due to the hydrogen charging and the minor influence of hydrogen to the UTS and YS. At hydrogen concentration of around 4.5 ml/100 g Fe, the CGHAZ showed distinct intergranular cracking accompanied by a distinct loss of UTS and YS.

The maximum charged hydrogen concentration of above 8 ml/100 g Fe (Fig. 19) changes the fracture topography for the WM to dominant cleavage fracture (regions marked with dashed red lines in upper part of Fig. 19). Compared to lower hydrogen concentrations, the degradation of the mechanical properties is similar. But, the changing fracture topography to "CF" in combination with the very low ductility indicates that at larger hydrogen concentrations, there should be a significant degradation effect. From this point of view, the weld metal is assumed to be less susceptible for hydrogen-related degradation of mechanical properties than the CGHAZ.

As a specific observation of the WM fracture surfaces, quasi-cleavage fracture occurred specifically around inclusions with characteristic cubic shape (as shown in Fig. 20a - indicated with a red arrow), exhibiting well-known fish-eye appearance.

As described in Fig. 20, the EDX spectrum indicates that the inclusion has a Ti-rich chemical composition (indicated with a red arrow in Fig. 20b). Including the inclusion and the obtained quasi-cleavage areas, it is assumed that the Ti-rich inclusions are the initial points for the forming of the embrittled areas in hydrogen charged condition under load. In general, this effect is well-known in steel grades and is called "fish-eye" and indicates a typical hydrogen degradation effect [40, 42]. Liua et al. [43] reported for Ni-bearing CrMoV steel embrittled areas around inclusions too. They conclude that the determined inclusions (no chemical composition given) were initiation points for the embrittled regions. According to Lynch [41] and Martin et al. [42], quasi-cleavage fracture ("C") is described by noncleavage planes with fine lines called river markings.
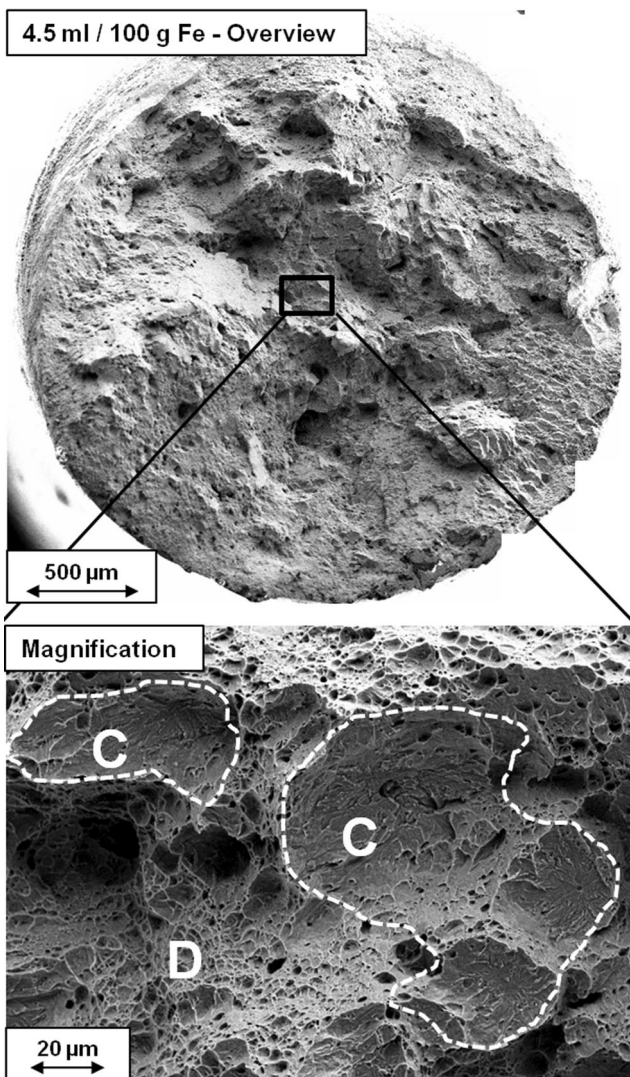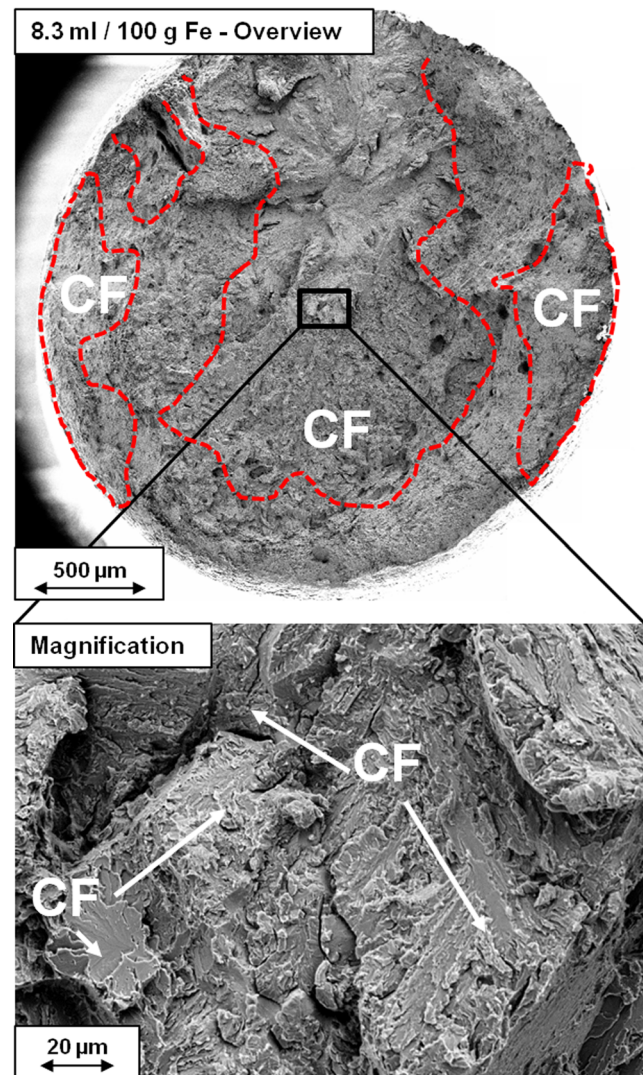
Fig. 18  WM charged with 4.5 ml/100 g Fe



Fig. 19  WM charged with 8.3 ml/100 g Fe

Similarly to the CGHAZ, it was observed that with increasing hydrogen concentration, the ratio of embrittled area and ductile area in the WM changes. In other words, with increasing hydrogen concentration in the WM, the embrittled area increases and the diameter after fracture increases, and the reduction in area changes. But, due to the remaining part of ductile fracture area, the WM shows slight better performance at higher hydrogen concentrations (>4.5 ml/100 g Fe) compared to CGHAZ. The occurred "fish-eyes" only formed in the WM. The initial point was assumed to be at the Ti-rich inclusions. Due to the peak temperature of the CGHAZ cycle (1200 °C), the Ti-rich inclusion is perhaps partly dissolved in the CGHAZ, and the quasi-cleavage cracking around these inclusions does not occur in the case of CGHAZ. Fish-eyes in the pure WM (TIG) were also reported by Pancikiewicz et al. [44]. Nevertheless, macroscopic fish-eyes are typically for previously hydrogen-charged specimens after tensile testing. Hence, a direct correlation of the Ti-rich inclusions as initiation point for the increasing degradation is very complex due to the multiaxial stress distribution in real welded components. Nevertheless, the tensile tests showed that the WM is less sensitive to macroscopic hydrogen-affected degradation (i.e., degradation of the ductility at high hydrogen concentrations) compared to the CGHAZ. Assuming the (auto-) tempered condition of WM, this is in accordance with slow strain rate test (SSRT) findings of Hoffmeister and Boellinghaus [13] who showed that the as-quenched T24 HAZ is more susceptible to HAC compared to the (tempered) base material.
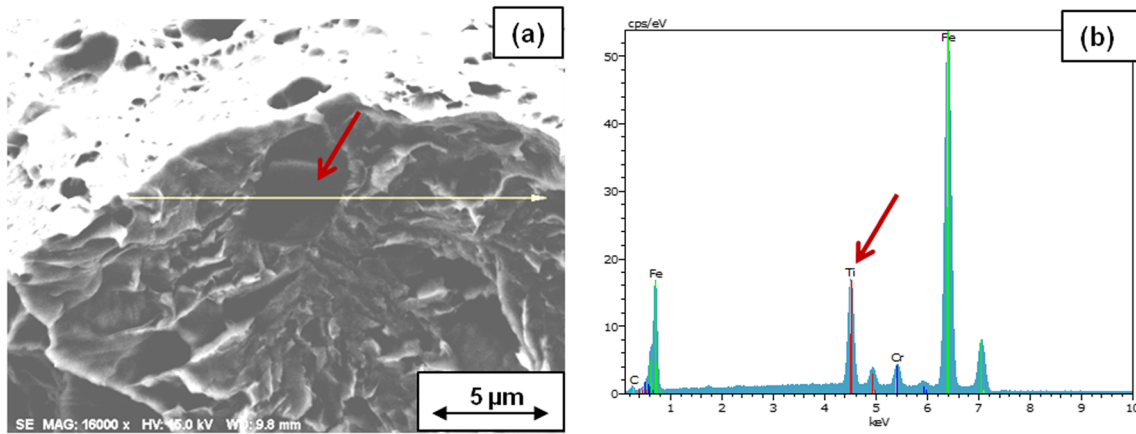
**Fig. 20** EDX at inclusion (**a**) and EDX spectrum (**b**)

### 3.5 Quantitative assessment of the hydrogen degradation effects

In contrast to the UTS or YS, the elongation at failure and the reduction in area are remarkably influenced in the presence of hydrogen in terms of degradation for both microstructures. Knowing the reduction in area from the initial cross section $A_0$ and the cross section after fracture $A_f$, one can calculate the true strain $\varepsilon_T$. The true strain is defined in Eq. 2: true strain [45].

$$\varepsilon_T = ln\left(\frac{A_0}{A_f}\right) \quad (2)$$

Using Eq. 2, the degradation of the reduction in area (true strain) can be expressed by a mathematic approximation using exponential functions as envelope curves for the plotted data. This procedure allows quantitative assessment and ranking of the different weld microstructures and their special susceptibility for hydrogen-related degradation. In addition, the envelope curves represent the influence of the local hydrogen

concentration and local mechanical load condition for the different microstructures. Figure 21 shows the envelope curves for the CGHAZ and Fig. 22 for the WM, respectively.

It is worth to see that the CGHAZ shows an increased loss of ductility compared to the weld metal expressed by the envelope curve especially for lower hydrogen concentrations. From this point of view, the CGHAZ is assumed to be more crack critical than the weld metal. The fitted envelope curves are given in the Table 6. Here, LC means lower envelope curve, UC means upper envelope curve, and HD represents the determined hydrogen concentration in milliliters/100 g Fe.

Such hydrogen-dependent material properties can be applied as a suitable cracking criterion in respective numerical analyzes [46, 47]. Thus, the numerical model has to show a sufficient resolution (mesh density) to account for the localized strain increase at the crack tips and also for the specific weld microstructure at the crack tip. Especially, the latter requires exact determination and application of the specific hydrogen-dependent material properties for each weld microstructure. Applying the data in such model, the numerical
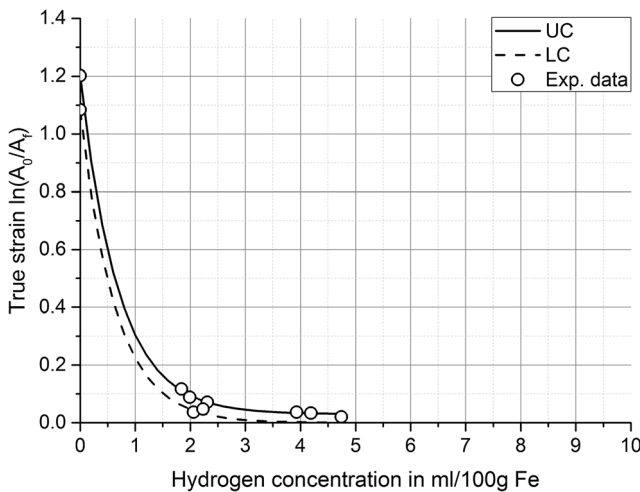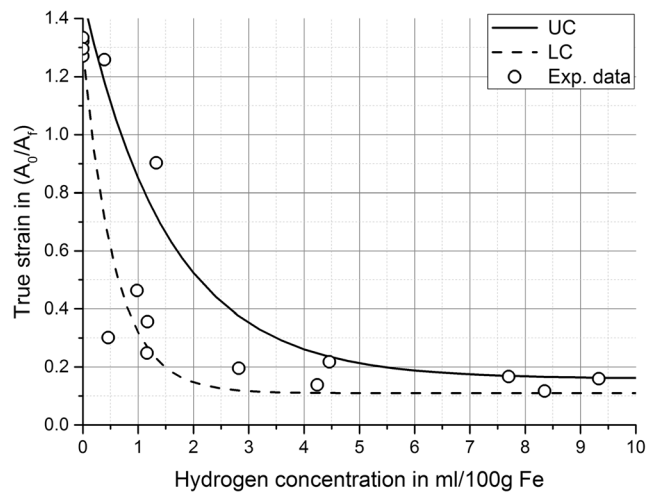


**Fig. 21** CGHAZ envelope curves



**Fig. 22** WM envelope curves

**Table 6** Envelope curves

| Grade | Approximation function |
| --- | --- |
| CGHAZ LC | $\varepsilon = 1.08 \times e^{-\frac{HD}{0.635}}$ |
| CGHAZ UC | $\varepsilon = 1.17 \times e^{-\frac{HD}{0.690}} - 0.03$ |
| WM LC | $\varepsilon = 1.18 \times e^{-\frac{HD}{0.578}} + 0.11$ |
| WM UC | $\varepsilon = 1.31 \times e^{-\frac{HD}{1.563}} + 0.16$ |

analysis gives information about the local strains and the hydrogen distribution resulting in potentially susceptible areas for degradation. Nevertheless, the HAC phenomenon is more complex (e.g., strain rate dependency, mechanical stress concentration factors, or interaction of the dislocations with the dissolved hydrogen) especially the crack nucleation. But, the direct experimental determination of a certain "crack critical" hydrogen concentration in front a crack tip is very difficult due to the correlation to specific weld microstructure features (i.e., hydrogen trapping). Hence, the suggested procedure of using a certain envelope curve represents an approach for the simplified numerical assessment of hydrogen-affected degradation effects (i.e., hydrogen-assisted cold cracking).

## 4 Conclusions

Tensile test was performed with uncharged and electrochemically hydrogen-charged specimens. T24 weld metal specimens were machined from TIG weld joints, and CGHAZ microstructure specimens were machined from base metal plates subjected to weld similar heat treatment. The specific hydrogen influenced degradation behavior of T24 WM, and CGHAZ was investigated by correlating the achieved hydrogen concentration to the mechanical properties. The corresponding dominant fracture topography was investigated by SEM. An attempt was made to assess the hydrogen-dependent mechanical properties by a mathematic approximation. The following conclusions can be drawn from this study:

- The achieved hydrogen concentration of the WM is by trend higher compared to the CGHAZ. Calibration specimens showed that the maximum hydrogen solubility of the WM is above 8 ml/100 g Fe and 4 to 5 ml/100 g for the CGHAZ. The higher hydrogen solubility of the WM is assumed to be influenced by changing hydrogen traps. In case of the WM, tempering effects of the three-layer technique can result in extensive precipitation of complex carbides in the WM, i.e., an increased number and density of hydrogen traps.
- In uncharged condition, the CGHAZ shows increased ultimate tensile strength (UTS) and yield strength (YS)

compared to the WM. This behavior is influenced by the higher hardness of the CGHAZ.

- In hydrogen-charged condition, the UTS and YS of both microstructures show a hydrogen influenced degradation. Thereby, the CGHAZ shows at hydrogen concentration of 4.5 ml/100 g Fe significant loss of the UTS (nearly zero ductility). Furthermore, the WM and CGHAZ show a distinct loss of ductility expressed by the loss of total elongation, the decrease of the reduction in area, and the calculated embrittlement index.
- The SEM investigation of the WM shows that with increasing hydrogen concentration, the fracture topography changes from ductile to a mixture of quasi-cleavage/ductile, in which Ti-rich inclusions are assumed to be the initiation points for brittle-related defects like the quasi-cleavage rosettes around the inclusions ("fish-eye forming"). Additionally, the cuboidal Ti-rich inclusions demonstrate the important role of precipitates/inclusions as possible hydrogen traps. At highest hydrogen concentration of 8 ml/100 g Fe cleavage fracture is the dominant fracture topography. The CGHAZ shows a change of the fracture topography from ductile to cleavage fracture for hydrogen concentration of 2 ml/100 g Fe and distinct intergranular cracking accompanied by secondary cracks at 4 ml/100 g Fe.
- Assessing the distinct loss of ductility at low hydrogen concentration, the CGHAZ shows a higher susceptibility to hydrogen-assisted degradation of the mechanical properties compared to the WM. A maximum hydrogen concentration of 2 ml/100 g Fe is recommended for avoidance of hydrogen degradation effects (HAC susceptibility respectively) at room temperature.
- The suggested envelope curves represent a method to assess the hydrogen-related degradation of the mechanical properties.

## References

1. Hahn B, Bendick W (2008) Rohrstaehle fuer moderne Hochleistungskraftwerke. 3R Int 47:3–12
2. Heuser H, Jochum C, Lecomte-Beckers J, Carton M, Schubert F, Ennis PJ (2002) Characterization of matching filler metals for new ferritic-bainitic steels like T/P 23 and T/P 24, Materials for Advanced Power Engineering 2002. Forschungszentrum Jülich, Jülich
3. Dhooge A, Vekeman J (2005) New generation 2¼Cr steels T/P 23 and T/P 24 weldabiltiy and high temperature properties. Weld World 49:75–93. doi:10.1007/bf03266492
4. Garet M, Brass AM, Haut C, Guttierez-Solana F (1998) Hydrogen trapping on non-metallic inclusions in Cr-Mo low alloyed steels. Corros Sci 40:1073–1086. doi:10.1016/S0010-938x(98)00008-0
5. Albert SK, Ramasubbu V, Parvathavarthini N, Gill TPS (2003) Influence of alloying on hydrogen-assisted cracking and diffusible hydrogen content in Cr-Mo steel welds. Sadhana 28:383–393. doi:10.1007/bf02706439

6. Coudreuse L, Bocquet P, Cheviet L (1992) Hydrogen trapping in Cr-Mo steels for hydro processing reactors. PVP-Vol. 239/ MPC- Vol. 33, Serviceability of Petroleum, Process and Power Equipment, ASME

7. Brouwer RC (1993) Hydrogen concentration distribution in the wall of pressure vessels made of conventional and V-modified steels. Int J Pres Ves Pip 56:133–148. doi:10.1016/0308-0161(93)90091-7

8. Brouwer RC (1992) Hydrogen diffusion and solubility in vanadium modified pressure vessel steels. Scripta Metall Mater 27:353–358. doi:10.1016/0956-716x(92)90525-j

9. Nowack R, Goette C, Heckmann S (2011) Quality management at RWE using T24 boiler material as an example (in German). VGB Powertech J 11:1–5

10. Boewe J, Becker M (2013) Modified commissioning procedure for USC boilers using material T24., Hitachi Power Europe GmbH Germany, http://pennwell.websds.net/2013/vienna/pge/papers/T4S5O3-paper.pdf. Accessed on 27 November 2014

11. Husemann RU, Devrient S, Kilian R (2012) Cracking mechanism in high temperature water-T24 Root cause analysis program. In: NN 38th VDI-Jahrestagung Schadensanalyse in Kraftwerken. VDI-Wissensforum, Düsseldorf, pp 87–103

12. Luedenbach G (2012) Stress corrosion cracking of T24. VGB Powertech. http://www.vgb.org/en/hv_12_presentations-dfid-47601.html. Accessed on 24 Mai 2014

13. Hoffmeister H, Boellinghaus T (2014) Modeling of combined anodic dissolution/hydrogen-assisted stress corrosion cracking of low- alloyed power plant steels in high-temperature water environments. Corros Sci 70:563–578. doi:10.5006/1048

14. Baeumel A, Drotden P, Pirchner H, Wagner G (1983) Study of stress corrosion cracking on welded high-strength fine grained structural steels in boiled feed water. Stahl Eisen 103:1091–1096

15. Nevasmaa P, Laukanen A (2005) Assessment of hydrogen cracking risk in multipass weld metal of 2.25Cr-1Mo-0.25V-TiB (T24) boiler steel. Weld World 49:45–58. doi:10.1007/bf03263423

16. Mohyla P, Foldyna V (2009) Improvement of reliability and creep resistance in advanced low-alloy steels. Mat Sci Eng A-Struct 510–511:234–237. doi:10.1016/j.msea.2008.05.056

17. Blach J, Falat F, Sevc P (2011) The influence of hydrogen charging on the notch tensile properties and fracture behavior on dissimilar weld joints of advanced Cr-Mo-V and Cr-Ni-Mo creep resistant steels. Eng Fail Anal 18:485–491. doi:10.1016/j.engfailanal.2010.09.043

18. Dayal RK, Parvathavarthini N (2003) Hydrogen embrittlement in power plant steels. Sadhana 28:431–451. doi:10.1007/bf02706442

19. Zimmer P, Seeger DM, Boellinghaus T, Cerjak H (2005) Hydrogen permeation and related material properties of high strength steels, High strength steels for hydropower plants - Proceedings. Institute for Materials Science, Welding and Forming, Graz, pp 1–18, paper-no 17

20. Heuser H (2009) Schweißtechnische Verarbeitung neuer Kraftwerkstähle. Forum-Schweißtechnik im Kraftwerksbau (SLV München). http://www.bayern-innovativ.de/schweisstechnik2009/download/heuser.pdf. Accessed 20 May 2014

21. Michler T, Naumann J (2010) Microstructure aspects upon hydrogen environment embrittlement of various bcc steels. Int J Hydrog Energ 35:821–832. doi:10.1016/j.ijhydene.2009.10.092

22. Salmi S, Rhode M, Juettner S, Zinke M (2015) Hydrogen determination in 22MnB5 steel grade by use of carrier gas hot extraction technique. Weld World 59:137–144. doi:10.1007/s40194-014-0186-z

23. Kannengiesser T, Tiersch N (2010) Measurements of diffusible hydrogen contents at elevated temperatures using different hot extraction techniques - an international round robin test. Weld World 54(5):R115–R122. doi:10.1007/BF03263497

24. Coudreuse L, Bocquet P (1995) Hydrogen diffusion and trapping in Cr-Mo steels for hydrotreating reactors. In: Turnbull A (ed) Hydrogen cracking in metals. The Institute of Materials, London, pp 227–239

25. Brass AM, Guillon F, Vivet S (2004) Quantification of hydrogen diffusion and trapping in 2.25Cr-1Mo and 3Cr-1Mo-V steels with electrochemical permeation technique and melt extraction. Metall Mater Trans A 35:1449–1464. doi:10.1007/s11661-004-0253-y

26. Takahashia J, Kawakamia K, Taruib T (2012) Direct observation of hydrogen-trapping sites in vanadium carbide precipitation steel by atom probe tomography. Scripta Mater 67:213–216. doi:10.1016/j.scriptamat.2012.04.022

27. Depover T, Monbaliu O, Wallaert E, Verbeken K (2015) Effect of Ti, Mo and Cr based precipitates on the hydrogen trapping and embrittlement of Fe-C-X Q&T alloys. Int J Hydrog Energ. doi:10.1016/j.ijhydene.2015.06.157, In Press, Corrected proof

28. Parvathavarthini N, Saroja S, Dayal RK, Khatak HS (2001) Studies on hydrogen permeability of 2.25%Cr-1%Mo ferritic steel: correlation with microstructure. J Nucl Mater 288:187–196. doi:10.1016/S0022-3115(00)00706-6

29. Mohyla P, Foldyna V (2009) Improvement of reliability and creep resistance in advanced low-alloy steels. Mater Sci Eng A 510(511): 234–237. doi:10.1016/j.msea.2008.05.056

30. Boellinghaus T, Hoffmeister H, Dangeleit A (1995) A scatterband for hydrogen diffusion coefficients in micro-alloyed low carbon structural steels. Weld World 35(2):83–96

31. Liu Y, Wang M, Liu G (2013) Hydrogen trapping in high strength martensitic steel after austenitized at different temperatures. Int J Hydrog Energ 38:14364–14368. doi:10.1016/j.ijhydene.2013.08.121

32. Matsuoka S, Homma N, Tanaka H, Fukushima Y, Murakami Y (2006) Effect of hydrogen on the tensile properties of 900MPa-class JIS-SCM435 low-alloy-steel for use in storage cylinder of hydrogen station. J Jpn Inst Metals 70:1002–1011. doi:10.2320/jinstmet.70.1002

33. Birnbaum HK, Sofronis P (1994) Hydrogen-enhanced localized plasticity - a mechanism for hydrogen-related fracture. Mat Sci Eng A-Struct 176:191–202. doi:10.1016/0921-5093(94)90975-X

34. Coleman KK, Newell WF (2007) P91 and Beyond -Welding the new-generation Cr-Mo alloys for high-temperature service. Weld J 86:29–33

35. Xu H, Xia X, Hua L, Sun Y, Dai Y (2012) Evaluation of hydrogen embrittlement susceptibility of temper embrittled 2.25Cr-1Mo steel by SSRT method. Eng Fail Anal. doi:10.1016/j.engfailanal.2011.08.008

36. Depover T, Perez Escobar D, Wallaert E, Zermout Z, Verbeken K (2014) Effect of hydrogen charging on the mechanical properties of advanced high strength steels. Int J Hydrog Energ 39:4647–4656. doi:10.1016/j.ijhydene.2013.12.190

37. Eliaz N, Shachar A, Tal B, Eliezer D (2002) Characteristics of hydrogen embrittlement, stress corrosion cracking and tempered martensite embrittlement in high-strength steels. Eng Fail Anal 9: 167–184. doi:10.1016/S1350-6307(01)00009-7

38. Gojic M, Kosec L, Matkovic P (2003) Embrittlement damage of low alloy Mn-V steel. Eng Fail Anal 10:93–102. doi:10.1016/s1350-6307(02)00038-9

39. Nelson HG (1983) Hydrogen embrittlement. In: Briant CL, Banerji SK (eds) Treatise on materials science and technology, vol 25. Academic Press, New York, pp 275–359

40. Beghini M, Benamati G, Bertini L, Valentini R (1998) Effect of hydrogen on tensile properties of martensitic steels for fusion application. J Nucl Mater 9:1295–1299. doi:10.1016/S0022-3115(98)00162-7

41. Lynch SP (1984) A fractographic study of gaseous hydrogen embrittlement and liquid-metal embrittlement in a tempered-martensitic steel. Acta Metall Mater 32:79–90. doi:10.1016/0001-6160(84)90204-9

42. Martin ML, Fenske JA, Liu GS, Sofronis P, Robertson IM (2011) On the formation and nature of quasi-cleavage fracture surfaces in hydrogen embrittled steels. Acta Mater 59:1601–1605. doi:10.1016/j.actamat.2010.11.024

43. Liua Q, Irwantob B, Atrensa A (2013) The influence of hydrogen on 3.5NiCrMoV steel studied using the linearly increasing stress test. Corros Sci 67:193–202. doi:10.1016/j.corsci.2012.10.019

44. Pancikiewicz K, Zielinska-Lipiec A, Tasak E (2013) Cracking of high-strength steel welded joints. Adv Mater Sci 13(3):76–85. doi:10.2478/adms-2013-0013

45. Davies JR (2004) Tensile testing. ASM-International, Materials Park, Ohio, USA

46. Wongpanya P, Boellinghaus T, Lothongkum G, Hoffmeister H (2009) Numerical modeling of cold cracking initiation and propagation in S 1100 QL steel root welds. Weld World 53:R34–R43. doi:10.1007/bf03266701

47. Mente T, Boellinghaus T, Schmitz-Niederau M (2012) Heat treatment effects on the reduction of hydrogen in multi-layer high-strength weld joints. Weld World 56:26–36. doi:10.1007/bf03321362